DOI:10.1021/ic702471d

Inorganic Chemistry
Article

On an Electrode Modified by a Supramolecular Ruthenium Mixed Valence (Ru^{II}/Ru^{III}) Diphosphine-Porphyrin Assembly

Luis R. Dinelli,[†] Gustavo Von Poelhsitz,*[,‡] Eduardo E. Castellano,[§] Javier Ellena,[§] Sérgio E. Galembeck,[∥] and Alzir A. Batista*[,⊥]

[†]*Fundação Educacional de Barretos, CEP 14783-226, Barretos (SP), Brazil,* [‡]*Departamento de Química, Campus Catalão, Universidade Federal de Goiás, CP 56, CEP 75704-020, Catalão (GO), Brazil,* [§]*Instituto de Física de São Carlos, Universidade de São Paulo, CP 369, CEP 13560-970, São Carlos (SP), Brazil,* [∥]*Departamento de Química, Faculdade de Filosofia, Ciências e Letras de Ribeirão Preto, Universidade de São Paulo, 14040-901, Ribeirão Preto (SP), Brazil, and* [⊥]*Departamento de Química, Universidade Federal de São Carlos, CP 676, CEP 13565-905, São Carlos (SP), Brazil*

Received December 20, 2007

Three novel polymetallic ruthenium (III) *meso*-tetra(4-pyridyl)porphyrins containing peripheral "$RuCl_3$(dppb)" moieties have been prepared and characterized. The X-ray structure of the tetraruthenated {NiTPyP[$RuCl_3$(dppb)]$_4$} porphyrin complex crystallizes in the triclinic space group $P\bar{1}$. This structure is discussed and compared with the crystal data for the *mer*-[$RuCl_3$(dppb)(py)]. The {TPyP[$RuCl_3$(dppb)]$_4$} and {CoTPyP[$RuCl_3$(dppb)]$_4$} porphyrins were used to obtain electrogenerated films on ITO and glass carbon electrode surfaces, respectively. Such tetraruthenated porphyrins form films of a mixed-valence species {TPyP[Ru(dppb)]$_4$(μCl_3)$_2$}$_{2n}^{4n2+}$ and {CoTPyP[Ru(dppb)]$_4$(μCl_3)$_2$}$_{2n}^{4n2+}$ on the electrode surface. The modified electrode with {CoTPyP[$RuCl_3$(dppb)]$_4$} is very stable and can be used to detect organic substrates such as catechol.

Introduction

One of the most exciting developments in inorganic porphyrin chemistry over the past 15 years has been the elaboration of modified electrode assemblies.[1−8] The modified electrodes, and especially polymetallic porphyrins involved in multielectron transfer catalysis, have been employed with increasing interest in analytical and bioanalytical chemistry.[9−14] These electrodes, obtained by attaching metal complexes to the peripheral pyridyl residues of various *meso*-tetra (4-pyridyl) and more recently of 3-pyridyl porphyrinates, have also been used as efficient catalysts in multielectron transfer reactions, and depending on the central metallic ion inserted in the porphyrin ring, they may enhance either the catalytic reduction of O_2 or CO_2 or the oxidation of ascorbic acid, NO, or sulfite.[1−4,15−29] In general, these films are formed by dipping the electrode in a solution of the metalloporphyrin and then allowing it dry slowly, resulting in deposition of the

*To whom correspondence should be addressed. Tel.: +551633518285. Fax: +551633518350. E-mail: gustvon@catalao.ufg.br (G.V.P.); daab@power.ufscar.br (A.A.B.).

(1) Shi, C.; Anson, F. C. *J. Am. Chem. Soc.* **1991**, *113*, 9564–9570.
(2) Shi, C. N.; Anson, F. C. *Inorg. Chem.* **1992**, *31*, 5078–5083.
(3) Steiger, B.; Shi, C.; Anson, F. C. *Inorg. Chem.* **1993**, *32*, 2107–2113.
(4) Anson, F. C.; Shi, C. N.; Steiger, B. *Acc. Chem. Res.* **1997**, *30*, 437–444.
(5) D'Souza, F.; Hsieh, Y. Y.; Deviprasad, G. R. *Chem. Commun.* **1998**, 1027–1028.
(6) Quintino, M. S. M.; Araki, K.; Toma, H. E.; Angnes, L. *Talanta* **2008**, *74*, 730–735.
(7) Skeika, T.; Marcovicz, C.; Nakagaki, S.; Fujiwara, S. T.; Wohnrath, K.; Nagata, N.; Pessoa, C. A. *Electroanalysis* **2007**, *19*, 2543–2550.
(8) Gadamsetti, K.; Swavey, S. *Dalton Trans.* **2006**, 5530–5535.
(9) Chen, S. M. *J. Electroanal. Chem.* **1997**, *432*, 101–109.
(10) Papkovsky, D.; Uskova, M. A.; Ponomarev, G. V.; Korpela, T.; Kulmala, S.; Guilbault, G. G. *Anal. Chim. Acta* **1998**, *374*, 1–9.
(11) Chan, R. J. H.; Su, Y. O.; Kuwana, T. *Inorg. Chem.* **1985**, *24*, 3777–3784.
(12) Duarte, J. C. *Anal. Chim. Acta* **2008**, *612*, 29–36.
(13) Wang, Y. S. *Anal. Lett.* **2004**, *37*, 575–590.
(14) Biesaga, M. *Talanta* **2000**, *51*, 209–224.
(15) Araki, K.; Toma, H. E. *J. Coord. Chem.* **1993**, *30*, 9–17.
(16) Araki, K.; Toma, H. E. *J. Photochem. Photobiol., A* **1994**, *83*, 245–250.
(17) Araki, K.; Toma, H. E. *J. Chem. Res.* **1994**, 290–290.
(18) Araki, K.; Angnes, L.; Azevedo, C. M. N.; Toma, H. E. *J. Electroanal. Chem.* **1995**, *397*, 205–210.
(19) Araki, K.; Angnes, L.; Toma, H. E. *Adv. Mater.* **1995**, *7*, 554–559.
(20) Angnes, L.; Azevedo, C. M. N.; Araki, K.; Toma, H. E. *Anal. Chim. Acta* **1996**, *329*, 91–95.
(21) Azevedo, C. M. N.; Araki, K.; Angnes, L.; Toma, H. E. *Electroanalysis* **1998**, *10*, 467–471.
(22) Shi, C. N.; Anson, F. C. *Electrochim. Acta* **1994**, *39*, 1613–1619.
(23) Steiger, B.; Anson, F. C. *Inorg. Chem.* **1994**, *33*, 5767–5779.
(24) Shi, C. N.; Anson, F. C. *Inorg. Chem.* **1996**, *35*, 7928–7931.
(25) Steiger, B.; Anson, F. C. *Inorg. Chem.* **1997**, *36*, 4138–4140.
(26) Shi, C. N.; Anson, F. C. *Inorg. Chem.* **1998**, *37*, 1037–1043.
(27) Rea, N.; Loock, B.; Lexa, D. *Inorg. Chim. Acta* **2001**, *312*, 53–66.
(28) Toma, H. E.; Araki, K. *Coord. Chem. Rev.* **2000**, *196*, 307–329.
(29) Mayer, I.; Nakamura, M.; Toma, H. E.; Araki, K. *Electrochim. Acta* **2006**, *52*, 263–271.

Published on Web 4/29/2009

Scheme 1. (A) Structure of Compound **1** and (B) Structure of Compounds **2** (M = Ni) and **3** (M = Co)

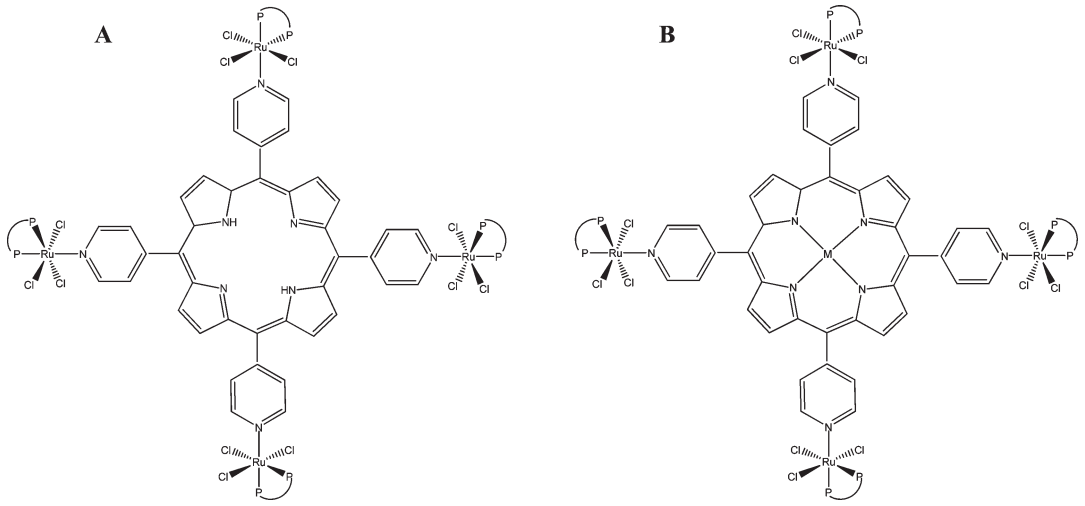

film on the electrode surface (dip-coating).[28,30−32] Previous work in these laboratories showed the possibility of obtaining a Langmuir−Blodgett (LB) film from mixtures of polyaniline and the *mer*-[$RuCl_3$(dppb)(py)] complex. This film was successfully utilized for dopamine detection.[33] Also, we showed that the tetraruthenated complex {TPyP[$RuCl_3$(dppb)]$_4$} was able to form Langmuir and LB films. These films were characterized by spectroscopic methods and used to modify electrodes for electrocatalysis.[34] Results indicated that the LB film of {TPyP[$RuCl_3$(dppb)]$_4$} was nanostructured and yielded an enhanced electrocatalytic activity for the oxidation of benzyl alcohol, compared to cast and electropolymerized films of the same compound.[34] Here, we describe a new technique to coat electrode surfaces using the "$RuCl_3$(dppb)" species that consists of generating electrochemically *in situ* a film of a ruthenium binuclear mixed-valence species. This is made possible by using the very specific unit "$RuCl_3$(dppb)"[35,36] attached to the peripheral pyridyl residues of the porphyrin ring.

Experimental Section

Materials. The chemicals employed were of reagent-grade quality (Aldrich). Tetrabutylammonium perchlorate (Fluka purum) was recrystallized from ethanol/water and dried overnight, under vacuum conditions, at 100 °C. Reagent-grade solvents (Merck) were appropriately distilled, dried, and stored over Linde 4 Å molecular sieves. Purified Ar was used in all procedures described herein for the removal of dissolved oxygen.

Physical Measurements. UV−vis spectra were recorded in CH_2Cl_2 on a Varian Cary 500 spectrophotometer. Electron paramagnetic resonance (EPR) spectra were measured at −160 °C with a Varian E-109 Instrument operating at the X-band frequency, within a rectangular cavity (E-248) fitted with a temperature controller. Cyclic voltammetry was carried out at room temperature in freshly distilled dichloromethane containing 0.1 mol/L $Bu_4N^+PF_6^-$ (TBAH) or 0.1 mol/L sodium trifluoracetate (NaTFA) solution, using an EG&G/PARC electrochemical system consisting of a 273A potentiostat or a BAS electrochemical analyzer. A three-electrode system with resistance compensation was used throughout. The working and auxiliary electrodes were stationary platinum foil and platinum wire, respectively. The reference electrode was Ag/AgCl in a Luggin capillary, 0.1 mol/L TBAH in CH_2Cl_2, a medium in which ferrocene is oxidized at 0.43 V (Fc^+/Fc). Elemental analyses were performed at the Department of Chemistry of the Federal University of São Carlos, São Carlos (Brazil), using a FISIONS CHNS, mod. EA1108 micro analyzer. Atomic-force microscopy (AFM) measurements were performed on an SPM Multimode-Nanoscope III from Digital Instruments, using the tapping mode. Suitable crystals for X-ray analyses were grown by slow evaporation of a dichloromethane−hexane solution of [$RuCl_3$(dppb)(py)] and {NiTPyP-[$RuCl_3$(dppb)]$_4$}.

Synthesis. The *mer*-[$RuCl_3$(dppb)(H_2O)] and *mer*-[$RuCl_3$-(dppb)(py)] [dppb = 1,4-bis(diphenylphosphino)butane and py = pyridine] complexes were synthesized following the published procedures.[35,36] The NiTPyP was synthesized by a modification of a procedure described in the literature:[37] 0.250 g (4.04×10^{-4} mol) of the 5,10,15,20-tetra(4-pyridyl)porphyrin (TPyP) and 0.254 g (1.01×10^{-3} mol) of nickel acetate were dissolved in a mixture of 20 mL of acetic acid and 20 mL of dimethylformamide under reflux. Yield: 272 mg (94%). Anal. calcd for $C_{40}H_{24}N_8Ni \cdot 2H_2O$: C, 67.53; H, 3.97; N, 15.75%. Found: C, 67.87; H, 3.64; N, 14.98%. UV−vis CH_2Cl_2, λ in nm ($\varepsilon \times 10^{-3}$ in L mol^{-1} cm^{-1}): 412 (70), 528 (7.5), 618 (4.1). The CoTPyP was synthesized as the NiTPyP, using 201 mg (8.08×10^{-4} mol) of cobalt(II) acetate and 250 mg (4.04×10^{-4} mol) of TPyP. Yield: 185 mg (68%). Anal. calcd for $C_{40}H_{24}N_8Co \cdot H_2O$: C, 69.26; H, 3.78; N, 16.15%. Found: C, 69.59; H, 4.17; N, 16.27%. UV−vis CH_2Cl_2, λ in nm ($\varepsilon \times 10^{-3}$ in L mol^{-1} cm^{-1}): 412 (44), 528 (6.2), 554 (4.8).

Synthesis of {TPyP[$RuCl_3$(dppb)]$_4$} (1). The {5,10,15,20-tetra(4-pyridyl)porphyrin-tetrakis(trichloro-1,4-bis(diphenylphosphino)butane)ruthenium(III)]} monomeric complex was

(30) Araki, K.; Winnischofer, H.; Viana, H. E. B.; Toyama, M. M.; Engelmann, F. M.; Mayer, I.; Formiga, A. L. B.; Toma, H. E. *J. Electroanal. Chem.* **2004**, *562*, 145–152.
(31) Winnischofer, H.; Lima, S. D.; Araki, K.; Toma, H. E. *Anal. Chim. Acta* **2003**, *480*, 97–107.
(32) Araki, K.; Wrighton, M. S.; Wagner, M. J. *Langmuir* **1996**, *12*, 5393–5398.
(33) Ferreira, M.; Dinelli, L. R.; Wohnrath, K.; Batista, A. A.; Oliveira, O. N. *Thin Solid Films* **2004**, *446*, 301–306.
(34) Wohnrath, K.; Dinelli, L. R.; Mello, S. V.; Constantino, C. J. L.; Leblanc, R. M.; Batista, A. A.; Oliveira, O. N. *J. Nanosci. Nanotechnol.* **2005**, *5*, 909–916.
(35) Dinelli, L. R.; Batista, A. A.; Wohnrath, K.; de Araujo, M. P.; Queiroz, S. L.; Bonfadini, M. R.; Oliva, G.; Nascimento, O. R.; Cyr, P. W.; MacFarlane, K. S.; James, B. R. *Inorg. Chem.* **1999**, *38*, 5341–5345.
(36) Wohnrath, K.; de Araujo, M. P.; Dinelli, L. R.; Batista, A. A.; Moreira, I. D.; Castellano, E. E.; Ellena, J. *J. Chem. Soc., Dalton Trans.* **2000**, 3383–3386.
(37) Fleischer, E. B. *Inorg. Chem.* **1962**, *1*, 493–495.

Table 1. Crystal Data and Structure Refinements for *mer*-[$RuCl_3$(dppb)(py)] and {NiTPyP[$RuCl_3$(dppb)]$_4$}

	mer-[$RuCl_3$(dppb)(py)]	{NiTPyP[$RuCl_3$(dppb)]$_4$}
empirical formula	$[C_{33}H_{33}Cl_3NP_2Ru]_2$	$\{[C_{38}H_{34}N_2P_2Cl_3Ru]_4Ni\}$ 1.7(CH_3OH).1.4(CH_2Cl_2).0.8(H_2O)
cryst syst	monoclinic	triclinic
space group	$C2/c$	$P\bar{1}$
fw	1425.93	3398.62
temperature, K	293(2)	100(2)
a, Å	32.194(3)	13.9380(5)
b, Å	11.0531(9)	16.7430(6)
c, Å	35.705(3)	19.9160(8)
β, deg	103.259(6)	α = 105.726(2) β = 94.509(2) γ = 109.108(2)
V (Å^3)	12366.7(17)	4155.1(3)
ρ_{calcd} (Mg/m^3)	1.532	1.358
μ (mm^{-1})	7.652	0.832
reflns collected	10917	22391
final R indices [$I > 2\sigma(I)$]	R1 = 0.0322, wR2 = 0.0842	R1 = 0.0669, wR2 = 0.1824

synthesized from 15 mg (2.24×10^{-5} mol) of TPyP (5,10,15, 20-tetra(4-pyridyl)porphyrin) and 65 mg (9.94×10^{-5} mol) of *mer*-[$RuCl_3$(dppb)H_2O] in 10 mL of a mixture of chloroform (95%) and methanol (5%). After the solution was stirred for 4 h, the volume was reduced under reduced pressure to about 2 mL and ether was added to give a reddish-brown powder. The excess of *mer*-[$RuCl_3$(dppb)(H_2O)] was removed by dissolution of the reaction product in CH_2Cl_2 followed by filtration. The filtrate was reduced to 1 mL, and ether was added to give the desired compound. Yield: 64.2 mg (84%). Anal. calcd for $C_{152}H_{138}N_8P_8Cl_{12}Ru_4$: C, 57.88; H, 4.41; N, 3.55%. Found: C, 57.53; H, 4.41; N, 3.58%. UV−vis CH_2Cl_2, λ in nm ($\varepsilon \times 10^{-4}$ in L mol^{-1} cm^{-1}): 228 (12), 254 (10), 422 (17), 514 (2.3), 544 (1.3), 584 (0.85), 642 (0.53).

Synthesis of {NiTPyP[$RuCl_3$(dppb)]$_4$} (2). This procedure is as described for **1** but uses 15 mg (2.20×10^{-5} mol) of the NiTPyP and 58 mg (9.04×10^{-5} mol) of *mer*-[$RuCl_3$(dppb)H_2O]. Yield: 65.2 mg (92%). Anal. calcd for $C_{152}H_{136}N_8P_8Cl_{12}NiRu_4$: C, 56.86; H, 4.27; N, 3.49%. Found: C, 56.31; H, 4.21; N, 3.30%. UV−vis CH_2Cl_2, λ in nm ($\varepsilon \times 10^{-4}$ in L mol^{-1} cm^{-1}): 238 (26), 250 (19), 420 (21), 540 (3.5), 612 (2.2).

Synthesis of {CoTPyP[$RuCl_3$(dppb)]$_4$} (3). This procedure is as described for **1** but uses CoTPyP (6 mg; 8.88×10^{-6} mol) and *mer*-[$RuCl_3$(dppb)(H_2O)] (23.1 mg; 3.55×10^{-6} mol). Yield: 21.0 mg (74%). Anal. calcd for $C_{152}H_{136}N_8P_8Cl_{12}CoRu_4$: C, 56.85; H, 4.27; N, 3.49%. Found: C, 56.73; H, 4.29; N, 3.46%. UV−vis CH_2Cl_2, λ in nm ($\varepsilon \times 10^{-4}$ in L mol^{-1} cm^{-1}): 236 (25), 252 (20), 444 (18), 554 (3.2), 600 (2.0).

X-Ray Crystallographic Data Collection, Refinement, and Description of the *mer*-[$RuCl_3$(dppb)(py)] and {NiTPyP[$RuCl_3$(dppb)]$_4$} Complexes. Crystallographic data of the *mer*-[$RuCl_3$(dppb)py] complex were collected on an Enraf-Nonius CAD-4 diffractometer with graphite-monochromated Cu Kα radiation (λ = 1.54184 Å). The final unit-cell parameters were obtained by least squares on the setting angles for 25 reflections with typical ranges of 2θ. Data were corrected for Lorentz and polarization effects and by absorption, using the method of Walker and Stuart.[38] Single crystals of the {NiTPyP[$RuCl_3$(dppb)]$_4$} complex were used for data collection and cell parameter determination on an Enraf-Nonius Kappa-CCD diffractometer, using Mo Kα radiation (λ = 0.71073 Å). Data collection for {NiTPyP[$RuCl_3$(dppb)]$_4$} was carried out with the *COLLECT* program;[39] integration and scaling of the reflections were performed with the HKL Denzo-Scalepack system of programs.[40] Absorption corrections were carried out using the multiscan method.[41] Both structures were solved by direct methods with *SHELXS*-97.[42] The models were refined by full-matrix least-squares on F^2 with *SHELXL*-97.[43] All of the hydrogen atoms were stereochemically positioned and refined with a riding model.[44]

Computational Methods. The crystallographic structures of *mer*-[$RuCl_3$(dppb)(py)] monomers and dimers were used without further refinement. The electron density was calculated by the B3LYP[45]/SDD[46,47] model. The intermolecular interactions were analyzed by the natural bond order (NBO) method[48] and by Wiberg bond indexes.[49] All of these calculations were made by the Gaussian 03 suite of software.[50] Figure 2 was generated by using the Molekel 5.3.0 program.

Results and Discussion

Complexes **1**−**3** were obtained in good yields utilizing mild conditions, as described previously in the Experimental

(38) Walker, N.; Stuart, D. *Acta Crystallogr., Sect. A* **1983**, *39*, 158–166.
(39) *Enraf-Nonius Collect*; Nonius BV: Delft, The Netherlands, 1997−2000.
(40) Otwinowski, Z.; Minor, W. Processing of X-ray Diffraction Data Collected in Oscillation Mode. In *Methods Enzymology, Macromolecular Crystallography*; Carter, J. C. W., Sweet, R. M., Eds.; Academic Press: New York, 1997; Vol. *276*, Part A, pp 307−26.
(41) Blessing, R. H. *Acta Crystallogr., Sect. A* **1995**, *51*, 33–38.
(42) Sheldrick, G. M. *SHELXS-97*; University of Gottingen: Gottingen, Germany, 1997.
(43) Sheldrick, G. M. *SHELXL-97*; University of Gottingen: Gottingen, Germany, 1997.
(44) Farrugia, L. J. *J. Appl. Crystallogr.* **1997**, *30*, 565.
(45) Becke, A. D. *J. Chem. Phys.* **1993**, *98*, 5648–5652.
(46) Andrae, D.; Haussermann, U.; Dolg, M.; Stoll, H.; Preuss, H. *Theor. Chim. Acta* **1990**, *77*, 123–141.
(47) Martin, J. M. L.; Sundermann, A. *J. Chem. Phys.* **2001**, *114*, 3408–3420.
(48) Weinhold, F. *Natural Bond Orbital Methods*; John Wiley & Sons: Chichester, U.K., 1998.
(49) Wiberg, K. B. *Tetrahedron* **1968**, *24*, 1083–1096.
(50) Frisch, M. J.; Trucks, G. W.; Schlegel, H. B.; Scuseria, G. E.; Robb, M. A.; Cheeseman, J. R.; Montgomery, J. A., Jr.; Vreven, T.; Kudin, K. N.; Burant, J. C.; Millam, J. M.; Iyengar, S. S.; Tomasi, J.; Barone, V.; Mennucci, B.; Cossi, M.; Scalmani, G.; Rega, N.; Petersson, G. A.; Nakatsuji, H.; Hada, M.; Ehara, M.; Toyota, K.; Fukuda, R.; Hasegawa, J.; Ishida, M.; Nakajima, T.; Honda, Y.; Kitao, O.; Nakai, H.; Klene, M.; Li, X.; Knox, J. E.; Hratchian, H. P.; Cross, J. B.; Adamo, C.; Jaramillo, J.; Gomperts, R.; Stratmann, R. E.; Yazyev, O.; Austin, A. J.; Cammi, R.;Pomelli, C.; Ochterski, J. W.; Ayala, P. Y.; Morokuma, K.; Voth, G. A.; Salvador, P.; Dannenberg, J. J.; Zakrzewski, V. G.; Dapprich, S.; Daniels, A. D.; Strain, M. C.; Farkas, O.; Malick, D. K.; Rabuck, A. D.; Raghavachari, K.; Foresman, J. B.; Ortiz, J. V.; Cui, Q.; Baboul, A. G.; Clifford, S.; Cioslowski, J.; Stefanov, B. B.; Liu, G.; Liashenko, A.; Piskorz, P.; Komaromi, I.; Martin, R. L.; Fox, D. J.; Keith, T.; Al-Laham, M. A.; Peng, C. Y.; Nanayakkara, A.; Challacombe, M.; Gill, P. M. W.; Johnson, B.; Chen, W.; Wong, M. W.; Gonzalez, C.; Pople, J. A. *Gaussian 03*, revision B.3; Gaussian, Inc.: Pittsburgh PA, 2003.

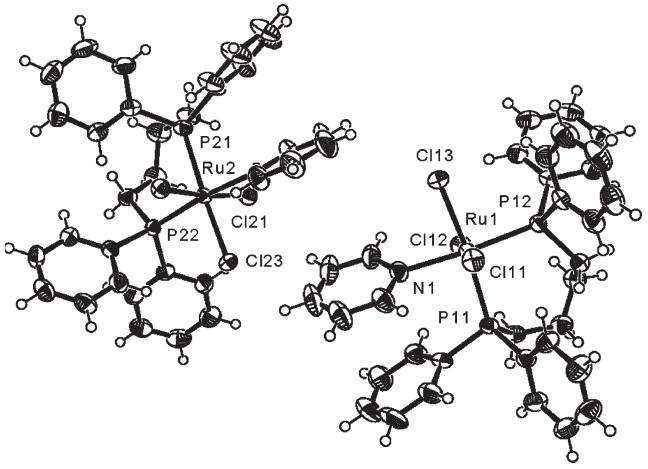

Figure 1. ORTEP[44] view of *mer*-[$RuCl_3$(dppb)(py)] showing the labeling scheme with 50% probability ellipsoids. Selected bond lengths (Å) and angles (deg): Ru(1)−N(1) 2.193(3), Ru(1)−Cl(11) 2.3304(8), Ru(1)−Cl(12) 2.3632(8), Ru(1)−Cl(13) 2.3807(9), Ru(1)−P(11), 2.4289(9), Ru(1)−P(12) 2.3325(8), Ru(2)−N(2) 2.220(3), Ru(2)−Cl(21) 2.3405(8), Ru(2)−Cl(22) 2.3410(8), Ru(2)−Cl(23) 2.3760(8), Ru(1)−P(21) 2.4025(9), Ru(2)−P(22) 2.3278(8); N(1)−Ru(1)−Cl(11) 87.97(8), N(1)−Ru(1)−P(12) 175.30(8), Cl(11)−Ru(1)−P(12) 91.82(3), N(1)−Ru(1)−Cl(12) 90.61(8), Cl(11)−Ru(1)−Cl(12) 177.83(3), Cl(11)−Ru(1)−Cl(13) 90.05(3), Cl(12)−Ru(1)−Cl(13) 91.45(3).

Section. Characterization data of these new species were in agreement with the proposed structures, indicating the presence of four peripheral "$RuCl_3$(dppb)" moieties. Scheme 1 shows the structures of these compounds. Crystals suitable for X-ray crystallography of *mer*-[$RuCl_3$(dppb)(py)] and {NiTPyP[$RuCl_3$(dppb)]$_4$} were obtained by the slow diffusion of hexane into a dichloromethane solution of the corresponding compounds. The crystallographic data and processing parameters are given in Table 1, and the ORTEP diagrams are shown in Figures 1 and 3, respectively.

The *mer*-[$RuCl_3$(dppb)(py)] complex crystallizes with two independent molecules per asymmetric unit in the $C2/c$ space group. The centers of the pyridine rings in the independent molecules are aligned to the center of a phenyl ring of the diphenylphosphine group, giving rise to a $\pi-\pi$ stacking interaction (see Figure 1). In molecule 1, the dihedral angle between the mean planes of the pyridine and the aromatic rings is 18.8(2)°. The distance between the centers of these two rings is 3.569(3) Å. In molecule 2, the angle between the mean ring planes is 23.0(2)°, and the distances between their centers is 3.703(3) Å. The dihedral angle between the two pyridine groups is 25.2(2)°, and their centers are separated by 4.722(3) Å. These numbers show that, in all cases, there is some degree of $\pi-\pi$ and van der Waals interactions, which are stronger between rings belonging to the same molecule.

Molecule 1 subtends a short contact with a symmetry-related molecule through a weak hydrogen bond between Cl13 and one aromatic hydrogen [Cl13−H114^{i} distance = 2.942(1)Å, Cl13−C114^{i} distance = 3.722(1)Å, i = 1/2 − x, y − 1/2, 1/2 − z]. Molecule 2 also subtends a short contact between Cl23 and the phenyl hydrogen of C255 [Cl23−H255^{ii} distance = 2.815(1)Å, Cl23−C255^{ii} = distance 3.662(1)Å, ii = 1/2 − x, 3/2 − y, −z]. These interactions are weak but not completely negligible, as shown by the calculation below. Together with the van der Waals interactions, they stabilize the packing arrangement. Further $\pi-\pi$ interactions are discarded due to the unfavorable angle between corresponding pyridine or phenyl rings.

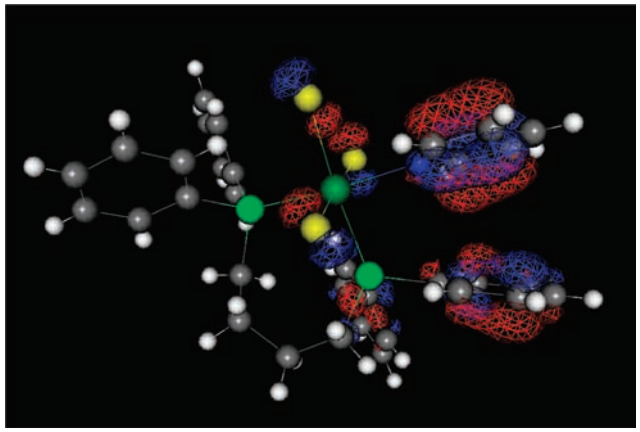

Figure 2. An occupied molecular orbital of *mer*-[$RuCl_3$(dppb)(py)] suggesting $\pi-\pi$ stacking interaction between the pyridine and aromatic rings of the phenyl groups.

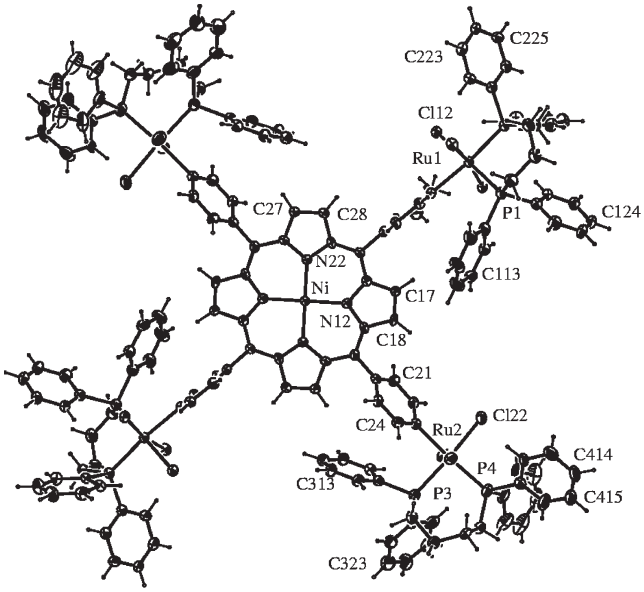

Figure 3. ORTEP[44] view of {NiTPyP[$RuCl_3$(dppb)]$_4$} showing the labeling scheme with 50% probability ellipsoids. Selected bond lengths (Å) and angles (deg): Ni−N(22)^{i} 1.955(6), Ni−N(12)^{i} 1.955(7), Ru(1)−N(11) 2.244(7), Ru(2)−N(21) 2.217(7), Ru(1)−Cl(11) 2.335(3), Ru(1)−Cl(12) 2.383(2), Ru(1)−Cl(13) 2.336(3), Ru(1)−P(1) 2.389(2), Ru(1)−P(2) 2.332 (2), Ru(2)−N(21) 2.217(7), Ru(2)−P(4) 2.336(3), Ru(2)−Cl(21) 2.339(3); N(11)−Ru(1)−Cl(11) 85.8(2), N(11)−Ru(1)−P(2) 173.29(19), P(2)−Ru (1)−Cl(11) 94.11(9), P(2)−Ru(1)−Cl(13) 94.60(9), Cl(11)−Ru(1)−Cl(13) 169.53(8), Cl(11)−Ru(1)−Cl(12) 92.10(8), Cl(13)−Ru(1)−Cl(12) 93.97 (9), P(2)−Ru(1)−P(1) 92.58(8), Cl(12)−Ru(1)−P(1) 178.86(9).

An intermolecular interaction between hydrogen H112 of molecule 1 and Cl23 of molecule 2 [Cl23−H112 distance = 2.923(1) Å, Cl23−C112 distance = 3.719(1)] links the parallel chains to the dimers. Examples of CH···ClM intermolecular interactions in the solid state have been recognized for some time.[51]

In order to assess the intra- and intermolecular interactions observed by X-ray crystallography of *mer*-[$RuCl_3$(dppb)(py)], electronic structure calculations were made. Some of the occupied molecular orbitals suggest a $\pi-\pi$ stacking

(51) Desiraju, G. R.; Steiner, T., *The Weak Hydrogen Bond*; Oxford University Press: New York, 1999.

Table 2. Data for Cl···H−C Hydrogen Bonds for [$RuCl_3$(dppb)(py)]

donor	acceptor[a]	$E^{(2)}$/kcal*mol^{-1}	b.i.[b]
π(Cl13)	σ*(C114^{i}−H114^{i})	0.28	0.0029
π(Cl23)	σ*(C255^{ii}−H255^{ii})	0.38	0.0031
π(Cl23)	σ*(C112−H112)	0.34	0.0033

[a] $i = 1/2 - x, y - 1/2, 1/2 - z$; $ii = 1/2 - x, 3/2 - y, -z$; $E^{(2)}$ = second-order energy stabilization. [b] b.i. = Wiberg bond index.

interaction between the pyridine and one ring of the diphenylphosphine group, as can be observed in Figure 2. An analysis of occupied molecular orbitals to verify through-bond interactions was used by Caramori and Galembeck[52,53] and by Grimme[54] in the study of [2,2]cyclophanes. The hydrogen bond between monomers was studied by the NBO method[49] and Wiberg bond indexes (b.i.).[50] In this first method, the existence of a X···H−Y hydrogen bond is indicated by the overlap of the X lone pair, n_π(X), with the σ antibonding orbital of the X−H bond, σ*(X−H). Part of the two electrons of n_π(X) is donated to σ*(X−H), stabilizing the system by the second-order energy stabilization, $E^{(2)}$. This method was widely used for the study of hydrogen bonds in several different systems.[55] Table 2 presents the bond indexes (b.i.) and $E^{(2)}$ values for all three intermolecular Cl···H−C interactions observed in the [$RuCl_3$(dppb)(py)] complex and mentioned above in the crystallographic data discussion. Both the stabilization and bond indexes indicate that this complex presents a week Cl···H−C hydrogen bond. The Cl···H−C intra- or intermolecular hydrogen bond was observed for several systems, as in the anti-AIDS compound, TIBO,[56] or in some metallic complexes, where the M−Cl···C−H was observed (M = metal).[57]

In the complex {NiTPyP[$RuCl_3$(dppb)]$_4$}, the Ni^{2+} ion is at the center of the porphyrin ring, bonded to the four nitrogen atoms in a planar configuration (see Figure 3). The porphyrin ring has four "$RuCl_3$(dppb)(py)" complexes as substituents, with the pyridyl rings roughly perpendicular to the plane of the porphyrin ring. This complex crystallizes in the $P\bar{1}$ space group with just one molecule per cell and the Ni atom sited at a center of symmetry. The structure is completed by a disordered dichloromethane group, a methanol, and a water solvent molecule (not shown in Figure 3). The distances between neighboring ruthenium ions are 14.30 (1) and 13.81(1) Å, and the entire molecule has an area of approximately 25.64(1) by 25.99(1) Å^2.

The porphyrin rings are stacked along the (2,−1,1) direction. The stacked molecules are linked through bifurcated intermolecular interactions between H424 and Ni and N12 of the molecules related by the symmetry operations $1 + x, 1 + y, z$ and $1 - x, 1 - y, -z$. The intermolecular interaction between the nickel cation and the CH bond were interpretated following Mukhopadhyay and Pal.[58] The crystal

Table 3. Intra- and Intermolecular Interactions in {NiTPyP[$RuCl_3$(dppb)]$_4$}

interaction[a]	A···H	A···D	H−D	A···H−D
Ni···H424^{i}−C424^{i}	2.767(9)	3.684(9)	0.95	162.5(3)
N12...H424^{i}−C424^{i}	2.681(9)	3.268(9)	0.95	120.6(3)
Cl23....H12W^{i}−O1W^{i}	2.614(9)	3.539(9)	0.95	164.9(3)
Cl22...H11W^{i}−O1W^{i}	2.573(9)	3.502(9)	0.95	166.2(3)
Cl11...H124^{ii}−C124^{ii}	2.858(8)	3.458(8)	0.95	122.0(4)
Cl11...H125^{ii}−C125^{ii}	2.762(8)	3.409(8)	0.95	126.2(4)

[a] Symmetry operations. $i = x + 1, y + 1, z$; $ii = -x, 1 - y, 1 - z$. Note: Sum of van der Waals radii: Ni + H = 3.5; N + H = 2.75; Cl + H = 2.95.

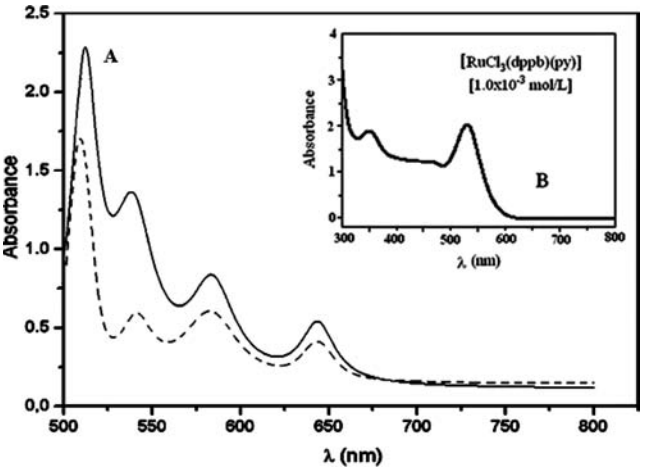

Figure 4. Electronic spectra of (A) (—) TPyP and (—) {TPyP[$RuCl_3$(dppb)]$_4$} [1.0×10^{-4} mol/L] and (B) *mer*-[$RuCl_3$(dppb)(py)] [1.0×10^{-3} mol/L] in CH_2Cl_2.

packing is stabilized, also, by the presence of two intermolecular interactions that give rise to the formation of infinite chains along the (110) direction (see Table 3). This interaction links two of the water molecules with two different Cl ions. Also, each molecule is linked to the molecules of a parallel chain, related by the symmetry operations $-x, 1 - y, 1 - z$ and $x, 1 + y, 1 + z$, by another bifurcated hydrogen bond between Cl11 and the aromatic hydrogen atoms H124 and H125. Each molecule is thus linked to four others, giving rise to an infinite supramolecular configuration. This molecular organization seems to be the first step in the electrochemical generation of the polymeric film that modifies the electrode properties, as described below.

Previously, we reported the electrochemistry of the *mer*-[$RuCl_3$(dppb)(py)] complex.[36] The controlled electrolysis of this complex produces the mixed-valence [Ru_2Cl_5(dppb)$_2$] species. This Ru^{II}/Ru^{III} complex is characterized by two intervalence transitions absorbing at 980 and 2050 nm and two reversible electrochemical processes ($Ru^{III}/Ru^{II} \rightarrow Ru^{III}/Ru^{III}$, $E_{1/2}$ = 0.70 V; $Ru^{III}/Ru^{II} \rightarrow Ru^{II}/Ru^{II}$, $E_{1/2}$ = 0.08 V).[36,59] Thus, the exhaustive electrolysis of the [$RuCl_3$(dppb)(py)] complex produces only the triply bridged compound [(dppb)RuCl(μ-Cl_3)Ru(py)(dppb)].[36] On the basis of this information, we have undertaken the study of a tetraruthenated porphyrin {TPyP[$RuCl_3$(dppb)]$_4$} to probe the possibility of forming a film of a mixed-valence species derived from this porphyrin on an electrode surface. The electronic

(52) Caramori, G. F.; Galembeck, S. E. *J. Phys. Chem A* **2007**, *111*, 1705–1712.
(53) Caramori, G. F.; Galembeck, S. E. *J. Phys. Chem. A* **2008**, *112*, 11784–11800.
(54) Grimme, S. *Chem. Eur. J.* **2004**, *10*, 3423–3429.
(55) Weinhold, F.; Landis, C. R. *Valency and Bonding: A Natural Bond Orbital Donor-Acceptor Perspective*; Cambridge University Press: Cambridge, U.K., 2005.
(56) Freitas, R. F.; Galembeck, S. E. *J. Phys. Chem. B* **2006**, *110*, 21287–21298.
(57) Aakeroy, C. B.; Evans, T. A.; Seddon, K. R.; Palinko, I. *New J. Chem.* **1999**, *23*, 145–152.
(58) Mukhopadhyay, A.; Pal, S. *Eur. J. Inorg. Chem.* **2006**, *23*, 4879–4887.
(59) Thorburn, I. S.; Rettig, S. J.; James, B. R. *Inorg. Chem.* **1986**, *25*, 234–240.

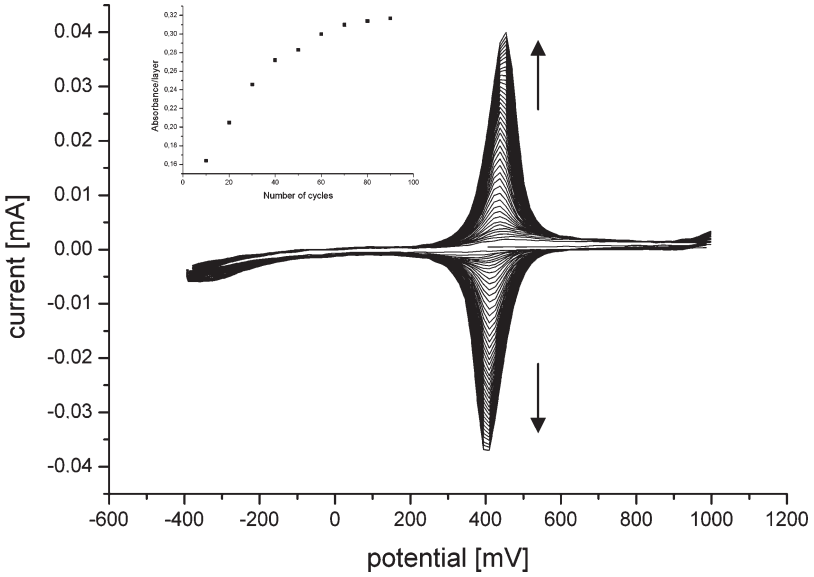

Figure 5. Repetitive voltammetric sweeps (90 cycles) of {TPyP[$RuCl_3$(dppb)]$_4$} (1×10^{-4} mol/L, 0.1 mol/L TBAH, CH_2Cl_2, ITO as working electrode and Ag/AgCl as reference electrode, 100 mV/s).

spectra of TPyP and {TPyP[$RuCl_3$(dppb)]$_4$} are very similar (Figure 4).

The absorption band at 544 nm of the tetrametalated compound is stronger than that of the free porphyrin, due to the contribution of the "$RuCl_3$(dppb)(py)" moiety of the porphyrin complex, since the [$RuCl_3$(dppb)py] complex strongly absorbs at 530 nm (Figure 4B).[36] Repetitive voltammetric sweeps between −400 mV and + 1000 mV, at a sweep rate of 100 mV/s, with a 10^{-4} mol/L solution of the {TPyP[$RuCl_3$(dppb)]$_4$} monomer (electrolyte = 0.1 mol/L TBAH in CH_2Cl_2 solution, ITO as the working electrode, and Ag/AgCl as the reference electrode) results in the behavior shown in Figure 5. The plot of the number of cycles in the cyclic voltammogram against the absorbance of the film increases almost linearly until about 60 cycles, after which there is a saturation of the ITO electrode (practically no more significant increase in absorbance, Figure 5, insert). The same behavior in the graphic is seen when the absorbance is plotted against the area of the cyclic voltammogram. After saturation of the ITO electrode (no further increase in current), a gold-colored and stable film was observed on the surface of the electrode. It's interesting to point out that, when the same film was generated in the TBAP electrolyte solution, it was not stable due to its solubility in this environment. This different behavior depending of the electrolyte suggests that the counterion, perchlorate for the TBAP and hexafluorphosphate for the TBAH, participates in the formation of the porphyrin film percolating into it. In this case, the PF_6^- better stabilizes the formed film on the electrode surface.

The $E_{1/2}$ potential of this process is 443 mV. The cyclic voltammogram of this film, on a Pt electrode using the same conditions above, exhibits a half-wave potential for the electrochemical process at 436 mV.

It is noteworthy that the cyclic voltammetric response exhibited by the immobilized film contains only a single peak in a potential range near the formal potential of the mixed-valence [Ru_2Cl_5(dppb)$_2$] complex.[59] This voltammetric response indicates the presence of intermolecular interactions between the ruthenium units in the compound. The amount of the {TPyP[Ru(dppb)]$_4$(μCl_3)$_2$}$_2$(PF_6)$_8$ film on the ITO electrode surface was calculated by the difference of absorbance of the solution before and after 90 cycles, and it was found to be ca. 3.0×10^{-4} g/cm^3. The electronic spectrum of the same film on the ITO electrode shows two bands in the near-infrared region, at 1070 and 1650 nm, which is typical of intervalence transitions for Ru^{II}/Ru^{III} phosphine systems.[59] The similarity of the spectrum observed for the ITO film with that recorded for the binuclear [Ru_2Cl_5(dppb)$_2$] complex in solution in the near-infrared region (Figure 6) suggests the following mechanism for the formation of the film on the surface of the electrodes:

$$n\{\text{TPyP[RuCl}_3\text{(dppb)]}_4\} + n4e^- \rightarrow n\text{'TPyP[RuCl}_2\text{(dppb)]}_4\text{'} + 4nCl^- \quad (1)$$

$$n\{\text{TPyP[RuCl}_3\text{(dppb)]}_4\} + n\text{'TPyP[RuCl}_2\text{(dppb)]}_4\text{'} \rightarrow \{\text{TPyP[Ru(dppb)]}_4(\mu Cl_3)_2\}_{2n}^{4n2+} + 8nCl^- \quad (2)$$

The suggested mechanism of the formation of the film in the ITO electrode can be seen in Scheme 2.

A possible structure for the film formed on the electrode surface can be seen in Scheme 3 (Por = porphyrin ring).

To confirm that the ITO surface was covered by a film of the {TPyP[Ru(dppb)]$_4$(μCl_3)$_2$}$_{2n}^{4n2+}$ species, such a film was dissolved in CH_2Cl_2, and 2,2′-bipyridine was added to the solution. We expected to obtain the [$Ru^{II}Cl_2$(dppb)(2,2′-bipy)] and the [$Ru^{III}Cl_2$(dppb)(2,2′-bipy)]Cl complexes, which are the products of the reaction of the mixed-valence binuclear [Ru_2Cl_5(dppb)$_2$] complex with the 2,2′-bipyridine ligand. The $^{31}P\{^1H\}$ NMR spectrum of the solution obtained showed doublets at 42.9 and 31.0 ppm ($^2J_{P-P}$ = 33 Hz)[60] (see Figure S1, Supporting Information and the EPR spectrum

(60) Queiroz, S. L.; Batista, A. A.; Oliva, G.; Gambardella, M. T. P.; Santos, R. H. A.; MacFarlan, K. S.; Rettig, S. J.; James, B. R. *Inorg. Chim. Acta* **1998**, *267*, 209–221.

shown in Figure 7), thus supporting our assumption about the composition of the film.

As can be seen in Figure 5B, the absorbance of the film formed on the ITO surface (measured close to 450 nm) increases during the first 90 cycles, until a steady state is reached. On the basis of our previous study (see below), the response can be attributed to the adsorbed mixed-valence Ru^{II}/Ru^{III} species. It should be noticed that, after deposition of the first layer, the absorbance increases nonlinearly and the observed increments are consistently smaller until a plateau is reached. This is evidence that the amount of the material deposited directly onto the ITO surface is larger than the amount deposited in each cycle on the porphyrin film. Thus, even considering the very first measurements, the plot of the absorbance against the number of layers does not pass through the origin, as it would if these layers were totally equivalent.

The fact that only a single voltammetric wave is observed for the four-electron processes involved in reaction 1 indicates that the four-coordinated "$RuCl_3$(dppb)" and $\{TPyP[Ru(dppb)]_4(\mu Cl_3)_2\}_{2n}^{4n2+}$ release electrons at essentially the same potential. The EPR spectrum of $\{TPyP[RuCl_3(dppb)]_4\}$ is silent, confirming the presence of interactions between the metal centers in the complex. The EPR of the $[RuCl_3(dppb)(py)]$ monomer, where there is no interaction between metal centers, shows three g values ($g_1 = 2.928$, $g_2 = 2.037$, and $g_3 = 1.607$), which is consistent with the X-ray structure (Figure 1).

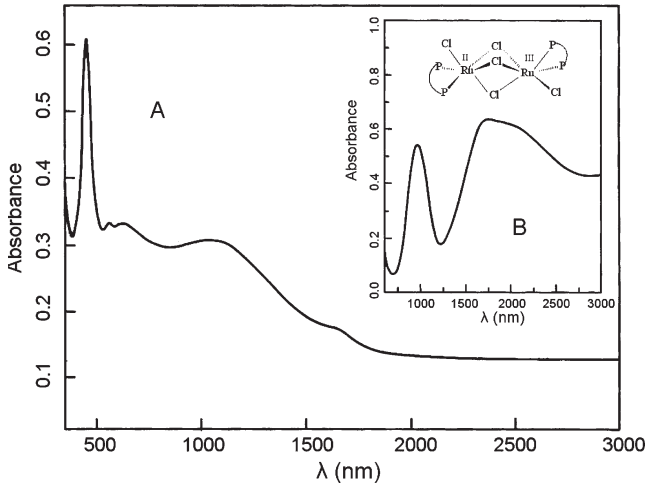

Figure 6. (A) Electronic spectrum of a film of $\{TPyP[Ru(dppb)]_4(\mu Cl_3)_2\}_{2n}^{4n2+}$ on an ITO surface in the visible and near-infrared regions. (B) Electronic spectrum of $[Ru_2Cl_5(dppb)_2]$ in CCl_4.

The cobalt porphyrin complex $\{CoTPyP[RuCl_3(dppb)]_4\}$ (**3**) was also synthesized and characterized. The electronic spectrum of **3** shows the following bands: Soret, 412 ($\varepsilon = 1.9 \times 10^5$ mol^{-1} cm^{-1}), 554 ($\varepsilon = 3.5 \times 10^4$ mol^{-1} cm^{-1}), and 610(sh) nm (2.0×10^4 mol^{-1} cm^{-1}). The film of this compound on the ITO surface shows transitions at 1054 and 1620 nm, confirming that also in this case the mixed-valence complex is formed on the electrode surface. Successive potential sweeps for the solution of **3**, using the same conditions applied for the $\{TPy[RuCl_3(dppb)]_4\}$ (see above), gave results similar to those shown in Figure 5, with $E_{1/2} = 448$ mV. This means that the cobalt(II) exerts almost no influence on the ruthenium reduction potential, probably due to the strong π-accepting character of the porphyrin ring. Atomic force microscopy in tapping mode was performed on the film of $\{CoTPy[RuCl_3(dppb)]_4\}$ formed on the ITO electrode surface. The thickness of the film layer formed after 90 cycles (Figure 8) was estimated to be about 84 nm and the roughness on the order of 18.439 nm for an area of 104.8 μm^2.

Considering the X-ray data for the *mer*-$[RuCl_3(dppb)(py)]$ complex and the fact that the minimum van der Waals cavity diameter of cobalt porphyrin is ca. 10 Å, it is reasonable to suggest that each electrochemical cycle deposits a single layer on the electrode surface, in which every two *trans* porphyrin rings are parallel to each other, bonding to different ruthenium atoms and perpendicular to the pyridyl rings. This suggestion is consistent with the fact that the *meso*-pyridyl group is roughly perpendicular to the porphyrin ring. Thus, this geometry promotes weak coupling between the redox centers, by minimizing overlap of the pyridyl and porphyrin π systems.[13] It is also possible that the imperfect homogeneity of the film is due to the cavity formed around the metal center in the film.

The stability of the modified electrode was verified in acidic and basic solutions (from 3.1 to 9.1 pH) and compared with nude platinum and glass electrodes, as shown in Figure 9. As can be seen, both the modified electrode and the glass electrode showed constant potentials after consecutives immersions in basic and acidic solutions. This was different from the nude platinum electrode, which showed a residual potential characterized by decreasing potential values after consecutive measurements.

The ability of the modified electrode to act as a potentiometric pH sensor was evaluated by a titration of the H_3PO_4 with NaOH, as shown in Figure 10. The modified electrode presented a higher sensitivity and stability when

Scheme 2. Suggested Mechanism of the Formation of the $\{TPyP[Ru(dppb)]_4(\mu Cl_3)_2\}_{2n}^{4n2+}$ Film on the ITO Electrode Surface

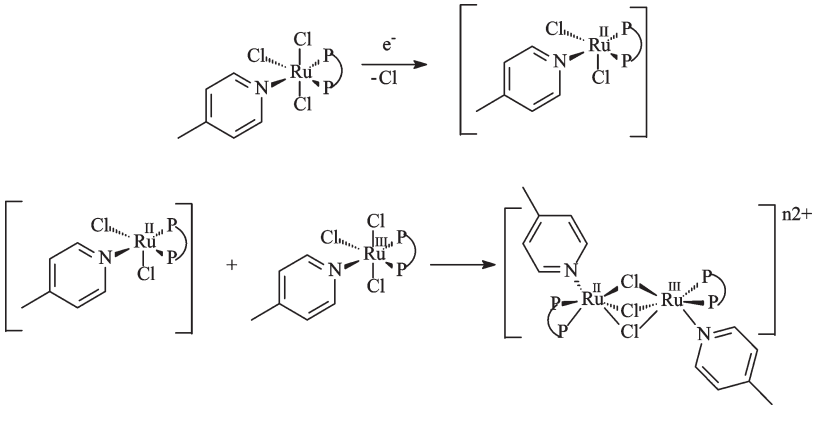

compared with the nude Pt electrode for the titration of H_3PO_4.

The electrode modified with the $\{CoTPyP[RuCl_3(dppb)]_4\}$ complex was used as a electrochemical sensor to detect the organic analyte catechol. As can be seen in Figure 11, the glass carbon modified electrode shows a better response than a nude carbon electrode. There is a shift of the oxidation potential from 341 mV (glass carbon electrode) to 188 mV, and the cyclic voltammogram is more reversible when it is modified. The cathodic shift is an advantage of the modified electrode when compared with the unmodified electrode due to the lesser influence of interferents.

The current intensity of the modified electrode is higher and better defined for the detection of the catechol substrate.

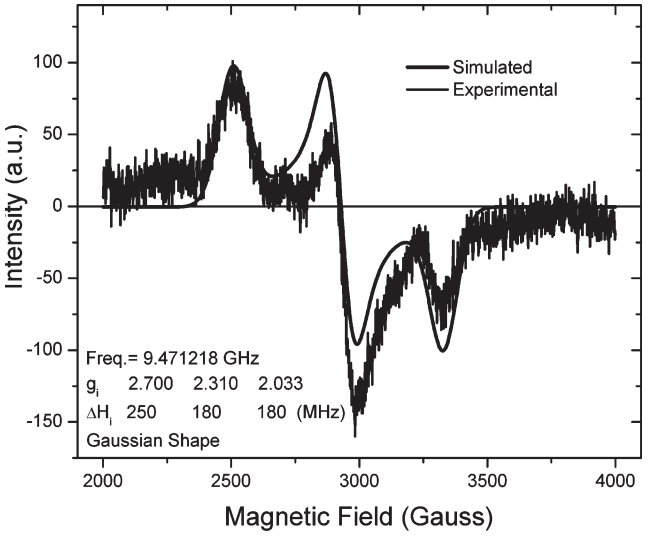

Figure 7. EPR spectrum of the $[RuCl_2(dppb)(2,2'\text{-bipy})]Cl$ in CH_2Cl_2 at −160 °C.

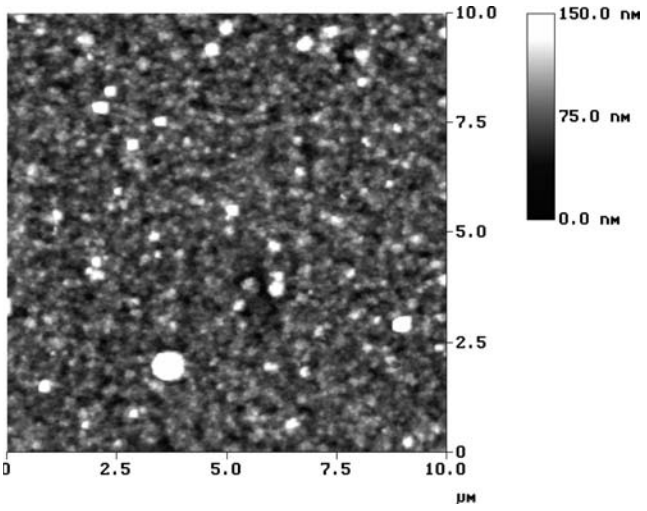

Figure 8. AFM image of a $\{CoTPyP[Ru(dppb)]_4(\mu Cl_3)_2\}_{2n}^{4n2+}$ film deposited on an ITO electrode surface.

Scheme 3. Suggested Structure of the $\{TPyP[Ru(dppb)]_4(\mu Cl_3)_2\}_{2n}^{4n2+}$ Film Formed on the ITO Electrode Surface

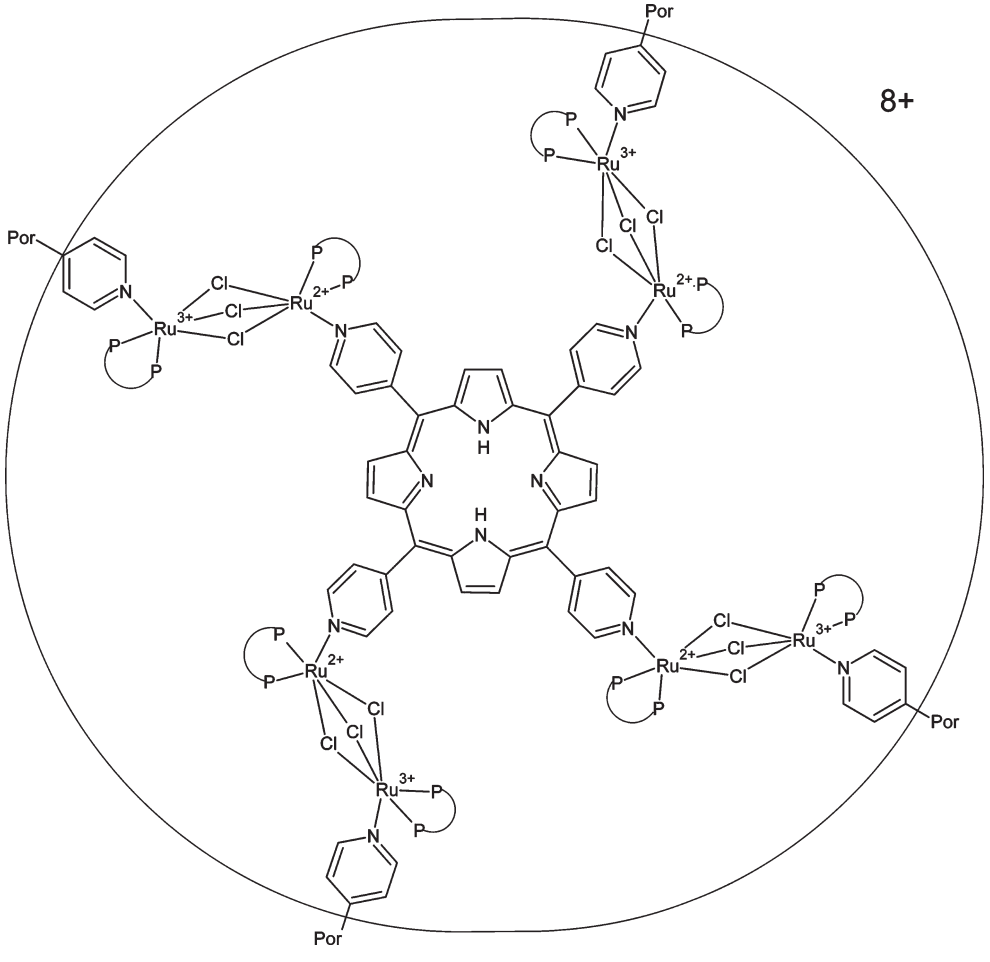

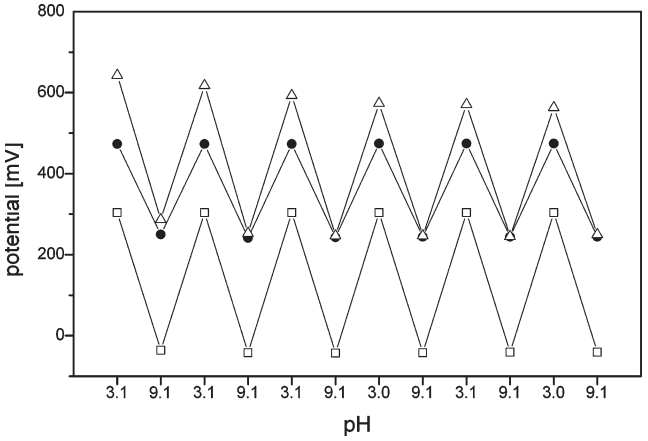

Figure 9. Stability of electrodes modified with {TPyP[Ru(dppb)]$_4$(μCl$_3$)$_2$}$_{2n}^{4n2+}$ (270 cycles): crude Pt (△); modified Pt (•), and glass (□) electrodes.

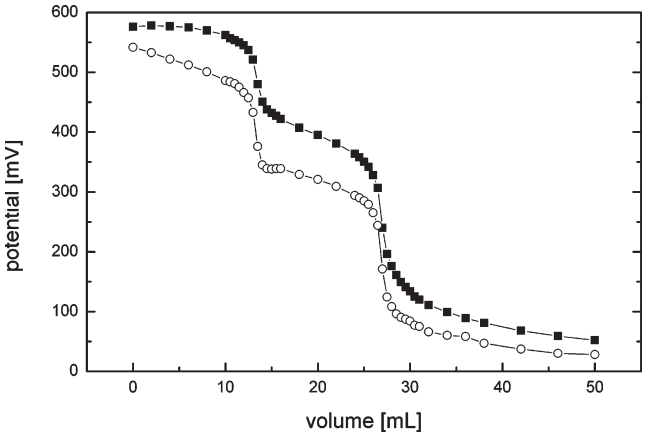

Figure 10. Titration of H_3PO_4 with Pt electrode modified with {TPyP[Ru(dppb)]$_4$(μCl$_3$)$_2$}$_{2n}^{4n2+}$ (270 cycles) (■) and nude Pt (○) electrode.

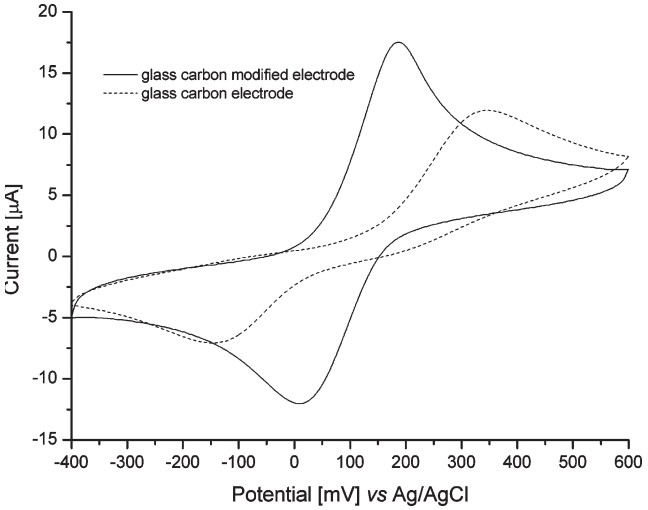

Figure 11. Cyclic voltamogram of a glass carbon electrode modified with {CoTPyP[Ru(dppb)]$_4$(μCl$_3$)$_2$}$_{2n}^{4n2+}$ using catechol as a test analyte (NaTFA 0.1 mol L^{-1}, pH = 4.5, sweep rate = 50 mV/s).

The electrode process involving one-electron oxidation is shown in Scheme 4.

Cyclic voltammograms of this process at several different concentrations of the substrate are shown in Figure 12. The analytical curve of the electrochemical process can be

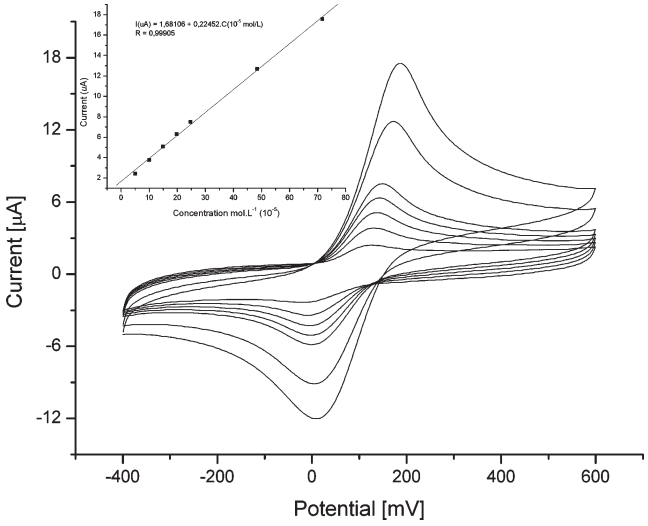

Figure 12. Cyclic voltammogram of the catechol substrate (conc. range: 5×10^{-5} to 1×10^{-3} mol L^{-1}). Film formed with {CoTPyP[Ru(dppb)]$_4$(μCl$_3$)$_2$}$_{2n}^{4n2+}$ on a glass carbon electrode vs Ag/AgCl (NaTFA 0.1 mol L^{-1}, pH = 4.5, sweep rate = 50 mV/s). Inset: Peak current plotted against concentration of analyte.

Scheme 4. Catechol Oxidation Showing Electron Delocalization

described by the following linear equation:

$$I_{ap}(\mu A) = 1.68106 + 0.22452 \times C\ (10^{-5}\ \text{mol L}^{-1})$$

The detection range used in the experiment was 5×10^{-5} to 1×10^{-3} mol L^{-1}. The limit of detection is about 1×10^{-5} mol L^{-1}.

Conclusions

Three novel polymetallic ruthenium(III) *meso*-tetra(4-pyridyl)porphyrins containing peripheral "RuCl$_3$(dppb)" moieties have been prepared and characterized. The X-ray structure of the tetraruthenated {NiTPyP[RuCl$_3$(dppb)]$_4$} porphyrin complex crystallizes in the triclinic space group $P\bar{1}$. The {TPyP[RuCl$_3$(dppb)]$_4$}, {NiTPyP[RuCl$_3$(dppb)]$_4$}, and {CoTPyP[RuCl$_3$(dppb)]$_4$} porphyrins can be used to obtain electrogenerated films on ITO and glass-carbon electrode surfaces. The organization of the structure of the metalloporphyrins seems to be the crucial step in the electrochemical generation of the polymeric film that modifies the electrodes. These tetraruthenated porphyrin films are suggested to be of the mixed-valence species {TPyP[Ru(dppb)]$_4$(μCl$_3$)$_2$}$_{2n}^{4n2+}$ and {MTPyP[Ru(dppb)]$_4$(μCl$_3$)$_2$]}$_{2n}^{4n2+}$ (M = Co or Ni) on the electrode surfaces. The electrode modified with {CoTPyP[Ru(dppb)]$_4$(μCl$_3$)$_2$}$_{2n}^{4n2+}$ is very stable and can be used to detect organic substrates such as catechol. The film containing cobalt gave a better response than the one with nickel in the detection of such organic substrates.

Acknowledgment. We thank CNPq, CAPES, FINEP, PRONEX, and FAPESP for financial support.

Supporting Information Available: Crystallographic data for *mer*-[RuCl$_3$(dppb)(py)] and {NiTPyP[RuCl$_3$(dppb)]$_4$} in CIF format and ^{31}P{^{1}H} NMR spectrum of *cis*-[RuCl$_2$(dppb)(bipy)]. This material is available free of charge via the Internet at http://pubs.acs.org.